SAND77-2052
Unlimited Release

DEPTH DISTRIBUTIONS OF LOW ENERGY DEUTERIUM IMPLANTATIONS IN (110) TUNGSTEN: A THEORETICAL MODEL

D. K. Brice

2900 Q(7-73)

ABSTRACT

The depth distributions of 80 eV D^+ implants in (110) W have recently been measured by field desorption microscopy. Prominent structure, consisting of seven major and several minor peaks, is observed in the measured distributions. This contrasts with conventional implantation theory which predicts two peaks, one for the channeled D^+ and one for the nonchanneled D^+ The observed structure is explained in the present report by a model which ascribes the various peaks to D^+ groups which have been scattered into planar channels by the surface impurities. The model allows a determination of D^+ stopping powers in the various planar channels and the stopping power of C and O impurities which recoil down the <110> axis. The model suggests that surface location of the impurities as well as their elastic scattering cross section for D^+ projectiles could be extracted from more elaborate calculations and experiments.

DEPTH DISTRIBUTIONS OF LOW ENERGY DEUTERIUM IMPLANTATIONS IN (110) TUNGSTEN: A THEORETICAL MODEL*

D. K. Brice
Sandia Laboratories, Albuquerque, NM 87185

Measurements of the depth distributions of atomic projectiles implanted into solids give information concerning the interactions between the projectiles and the target atoms. For relatively high energy implants the projectiles penetrate a considerable distance into the target material and only quantities which are related to averages over a large number of collision events are readily accessible from the measured depth profiles.[1] Such quantities include, for example, the average projected range of the incident projectiles, R_p, the standard deviation in R_p, ΔR_p, the standard deviation of the distribution transverse to the incident direction, etc. From such quantities as these the "average" properties of the projectile-host atom interaction can often be determined, such as the inelastic contribution to the stopping power and the ratio of elastic to inelastic interaction strengths.

Recently, Panitz (5114) has reported measurement of the depth distribution of low energy (~ 80 eV) deuterons implanted into (110) oriented tungsten with depth resolution of ~ 2.2 Å, i.e., the spacing of the (110)-W planes.[2] The precision of such measurements, along with the fact that the deuterons penetrate only a short distance into the target, clearly presents the possibility

*This work supported by the U. S. Department of Energy, DOE, under Contract AT(29-1)789.

of obtaining more detailed information relative to the incident ion-target atom interaction. In particular, on the basis of a model to be presented later in the report, it appears that the depth distribution of the deuterons is quite sensitive to the presence and location of surface impurities. This sensitivity is reflected in the complicated structure observed in the experimental distributions.

In the present report a semi-quantitative model will be presented which can account for the observed structure in the depth distributions. The model is presented in a semi-quantitative form at this time because the limited amount of experimental data available do not justify a more sophisticated approach. Further, certain predictions can be made with the semi-quantitative model which suggest additional experiments to validate the basic assumptions of the model. These additional experiments will provide data from which certain properties of the ion-target atom interaction can be extracted, and which will aid in refining the model. The quantities accessible to evaluation by the model of this report are 1) the energy dependences of the low energy channeling stopping power for the incident deuterons for the various "open" planar channels in the target, 2) the energy dependence of the deuteron stopping power in the <110> axial channel, 3) similar information for the recoil implanted surface impurities, and 4) the acceptance angle for channeling in the "open" planar channels. With a more sophisticated model, it should also be possible to evaluate the crystallographic location of the surface impurities on the target, as well as the deuteron-impurity atom elastic

scattering cross-section. As indicated above, however, the more sophisticated approach should await further experimental verification of the model in its present form.

In Section I of this report the existing experimental measurements will be briefly reviewed. Particular attention will be given there to indicating desirable refinements in the experiments as well as pointing out additional measurements which would be useful in verifying the theoretical model presented in subsequent sections. In Section II various models of projectile-target interactions which might conceivably lead to structure in the implanted projectile depth distribution (such as that observed in ref. 2) will be considered. The most promising of these models, the surface scattering-channeling model, will then be discussed in some detail. In Section III the semi-quantitative surface scattering-channeling model will be developed, and finally, in Section IV comparison between the model and the limited experimental data presently available will be presented.

I. EXPERIMENTAL

The reader is referred to reference 2 for details concerning the experimental apparatus and measurement techniques used in obtaining the low energy implanted deuterium depth profiles. Only those details pertinent to the present discussion will be reviewed here. The target for these implants consisted of a thin "needle" of tungsten single crystal, with a <110> crystallographic axis oriented parallel to the needle axis. The tip of the needle was rounded so that it consisted of a series of circular atomically

thin (110) plane platlets with increasing radius as one proceeds from the tip into the body of the needle. Prior to implantation the target surface was characterized and approximately a monolayer of carbon and oxygen impurities was found to be present. These impurities are characteristic of the residual gas in the target chamber. The D implants were made into the tip of the needle, at a nominal implant energy of 80 eV, and with the target at 300 K. No attempt was made to separate ions and neutrals from the D source prior to implantation.

After implantation the target was quickly transferred to the imaging field desorption spectrometer and cooled to 80 K for the depth distribution measurements. The depth distributions were then obtained by removing and analyzing the constituent atomic planes, atomic layer by atomic layer, through the method of imaging field desorption. The composition of each atomic layer was obtained during the removal process from time-of-flight measurements of the various atom and atom aggregates between the target and a collector.

Figure 1 shows typical results obtained in the measurements. There the implanted D distribution is seen to extend in to about 50 atomic layers with prominent structure appearing at depths of 11, 13, 16, 22, 33, and 46 atomic layers. Other minor structure is also seen in the D profile. The C and O impurities, which previously resided on the surface, are seen to have distributions extending to a depth of 10 atomic layers subsequent to the D implant. The total D contained in the profile of the figure amounts to approximately one monolayer. The results shown here are typical and reproducible.

fraction is reflected from the target surface, so that ultimately the random and channeled fractions within the target are in the ratio of approximately 1/6.

All of the above remarks concerning the separation of the channeled and random fractions are based on the conventional channeling theory which has been applied successfully to the channeling of high energy (100's of keV) projectiles. In this theory the correlated scattering of the channeled projectiles by the lattice atoms in the walls of the channel is replaced by a continuum model in which the channel walls are structureless, are parallel to the channel direction, and are the source of a potential energy function which governs the motion of the channeled projectiles transverse to the channel direction. In extending the concept of channeling to the lower energies of ref. 2 the continuum model clearly becomes questionable. The fundamental defining quality of the channeling phenomenon, i.e., a series of correlated collisions with wall atoms which gently steers the projectile along a trajectory between the channel walls, can however be retained. In fact the correlation in the low energy events need not be as high as for the high energy scattering since the low energy projectiles of ref. 2 only penetrate a few tens of lattice spacings into the target and probably traverse the channel only a few times before coming to rest. A more precise definition of the properties of low energy "channeled" projectiles will have to be postponed until a detailed examination of solutions to the equations of motion can be carried out.

Conventional theory can be applied to determine the profile of the random fraction, since the development of this profile is expected to be governed by random transport theory. These calculations have been performed using a previously described technique,[1] and with experimental stopping power values extrapolated down to the energy range of interest here. The results indicate that the random fraction should have a mean depth of penetration of 8.7 Å, with a standard deviation of 25.1 Å. These same calculations suggest that the channeled fraction should penetrate to a depth of ~ 157 Å.

The experimental results shown in Fig. 1 are in accord with the above general remarks on two accounts. First, approximately 15% of the implanted D ions are observed to occupy a broad peak near the target surface with a mean penetration depth of ~ 10 Å. Second, the D-depth distribution extends into the target to a maximum depth of ~ 115 Å, with a small peak in the distribution located at about 100 Å. Between these two peaks, which are tentatively identified as the channeled and nonchanneled groups, a multiplicity of D groups appear at well defined depths, contrary to the predictions of the conventional theory.

b) Structure Producing Effects

In attempting to explain the observed structure in Fig. 1 several different effects have been considered. These are: 1) the implanted D atoms diffuse to lattice damage or defects in the target and are trapped; 2) there is structure in the energy loss rate function for the D ions in the W target due to interactions with electrons having well-defined energy levels in the W; and 3) elastic scattering from impurity atoms at the target surface produces groups

of D ions which are channeled in planar channels not parallel with the original direction of motion.

Since the implants were performed at room temperature, and several minutes elapsed between the implant and the subsequent reduction of temperature to 80 K, the possibility of significant D diffusion clearly exists. The diffusion coefficient for D in W has not been measured, but the values for the diffusion coefficient in other materials[5] suggests that diffusion in W under the conditions of the reported experiments might cause D motion by some 10's or 100's of Angstroms. That this effect does not take place can be argued as follows: First, the D ions have insufficient energy to produce lattice damage in the target since the displacement threshold energy is 35 eV.[6] Thus for the effect to exist the "gettering" of the D would have to be at intrinsic defects. The reproducibility of the depth distributions in different targets rules this out, because the intrinsic defects would be expected to be randomly distributed. It thus appears that no significant diffusion of D in W occurs at room temperature over periods of several minutes duration.

The second effect mentioned above could also lead to structure in the observed D depth distributions with interactions occurring between the D ions and localized electrons in the W, or with plasmons. From the separation of the peaks in Fig. 1 the energy transfers in such interactions would be ~ 5 - 10 eV, and the interaction cross section would have to be quite large since most of the D ions are contained in peaks other than the "channeled" peak at the deep end of the distribution. The incident D ions have velocities

$\lesssim 10^7$ cm/sec while localized electrons with binding energies of several eV have orbital velocities $\gtrsim 10^8$ cm/sec. Therefore, the interaction cross section for interactions between the D ions and such electrons will be relatively low, since such cross sections become significant only when the D ion velocity is approximately equal to or greater than the electron velocity. Also, according to our present understanding of plasmons, the production rate for these excitations is quite small for D ion velocities significantly less than the Fermi velocity of the conduction electron gas, which is also $\sim 10^8$ cm/sec. Thus significant energy loss to well defined energy levels in the W target can be ruled out in the present case since the low velocity of the D ions leads to low cross sections for the (relatively) large energy transfers required to explain the observed structure.

The presence of impurity atoms on the W surface clearly leads to at least one additional group of D ions along with the random and channeled fractions mentioned earlier. This third group is that group of ions which scatter from the impurity atoms and suffer large angle deflections from the initial direction of motion. This group can be further subdivided according to whether the scattered ion is channeled or not in its new direction of motion. According to conventional theory, the scattered ion will be channeled in a new channel, c, providing that the new direction of motion is parallel to the channel direction within a critical angle, ψ_c, and providing that the scattering center does <u>not</u> lie in a row or plane of atoms parallel to the channel direction. It also seems reasonable to postulate the existence of a critical angle for

channeling in the low energy case, although its dependence on the various kinematic and crystallographic parameters may be more complex than in the higher energy case. The new channel could be either an axial or a planar channel, but planar channels will be much more likely since the axial channels subtend such small solid angles for acceptance of the scattered particles. In any case, the planar channel is a more general type of channel since axial channels may be thought of as simply the intersections of two or more planar channels. Thus, in the discussion which follows only planar channels will be considered, except for those ions initially channeled in the <110> direction.

The model suggested by the impurity scattering of the beam at the surface is then the following: Those ions scattered in directions within $\pm \psi_c$ of a given planar channel become channeled in a new direction, and thus do not penetrate as deeply into the target as the <110> channeled ions since their trajectory makes a large angle with respect to the initial direction of the motion. This is illustrated schematically in Fig. 2. The multiplicity of peaks in the observed distribution results from the large number of low index planar channels in the lattice at different and distinct scattering angles with respect to the initial direction of motion. The presence or absence of a peak associated with a given planar channel gives information on the location of the scattering center, since a given channel will be "blocked" if the scattering center lies in a plane of atoms parallel to that channel. This model will be developed more fully in the next section.

III. THE IMPURITY SCATTERING-CHANNELING MODEL

a) General

Consider a projectile of mass M_1, energy E, and velocity $\vec{v}$ to be incident on a target with $\vec{v}$ parallel to some low index crystallographic direction. Allow the particle to scatter from an atom of mass M_2 into the solid angle $d(\text{Cos }\theta)d\alpha$, where θ is the scattering angle and α is an azimuthal angle around the initial direction of motion. The probability that the scattered particle is channeled in the crystal plane c will be a function of θ, α, and E as well as the masses M_1 and M_2, and the crystallographic location, $\vec{r}$, of the scattering center. Let this probability be represented by $Q_c(\theta, \alpha, E, M_1, M_2, \vec{r})$. In the following discussion the dependence of Q_c on E, M_1, M_2, and $\vec{r}$ will be suppressed, although the reader should be aware that this dependence is present.

The differential cross section for scattering into the channel, c, at the angle θ is given by $d\sigma_c(\theta)$, where

$$d\sigma_c(\theta) = \sigma(\theta)\, d(\text{Cos }\theta) \int_0^{2\pi} Q_c(\theta, \alpha)d\alpha \qquad (1)$$

where it has been assumed that the elastic scattering cross section, $\sigma(\theta)$ is independent of the angle α. The quantity of interest for comparison with experiment is the depth distribution of the channeled particles after they have come to rest. Let $G_c(R)dR$ represent the probability that a particle scattered into the channel c comes to rest in the depth interval dR centered on R. If N is the areal density of the surface scattering centers then

$$G_c(R)dR = N\, d\sigma_c(\theta) \quad , \tag{2}$$

and a relationship between θ and R is needed to make a correspondence between the variables on the right and left hand sides of the equation. This correspondence is obtained through the stopping power of the ion in the channel.

It is assumed that the stopping power of the target for channeled particles can be written as

$$dE/dx = -S_c\, E^{p_c} \quad , \tag{3}$$

where the constants S_c and p_c are characteristic of the channel involved. It is further expected that $p_c \approx 0.5$.[7] If the scattered particle has energy T as it enters the channel, then Eq. (3) predicts that it will have a range $R_c(T)$ in the channel where

$$R_c(T) = F_c T^{1-p_c} \quad , \tag{4}$$

with

$$F_c = 1/S_c(1 - p_c) \quad . \tag{5}$$

Conservation of energy and momentum in the elastic scattering event gives T in terms of the initial energy E and the scattering angle θ through

$$T/E = K^2(\theta) \quad , \tag{6}$$

where

$$K(\theta) = A \cos\theta \pm (A^2 \cos^2\theta + B)^{1/2} \tag{7}$$

with

$$A = M_1/(M_1 + M_2) \tag{8a}$$

$$B = (M_2 - M_1)/(M_1 + M_2) \quad . \tag{8b}$$

For $M_2 > M_1$ only the positive square root is used in (7), while both signs are used for $M_1 > M_2$ and the T vs θ function becomes double valued. The former case applies to the experiments of interest here. From (4) and (6) one obtains

$$R_c(T) = F_c \, E^{1-p_c} \, K^{2-2p_c} \quad . \tag{9}$$

The variable R in Eq. (2) is, however, depth in the target rather than the range parallel to the planar channel. Thus, when R_c is projected onto the original direction of motion we obtain

$$R_{pc}(T) = F_c \, E^{1-p_c} \, K^{2-2p_c} \, \mathrm{Cos} \, \theta \tag{10}$$

which gives the desired relationship between $R = R_{pc}$ and θ for use in Eq. (2).

From Eq. (10) it is seen that each channel has its unique depth scale, determined by the constants S_c and p_c. The constants p_c should thus easily be determined from a series of experiments in which the incident projectile energy is varied since the peak depths for a given type of channel should vary as E^{1-p_c}.

For small acceptance angles the total depth distribution of the scattered-channeled particles should be given by G(R)dR, where

$$G(R) \approx \sum_c G_c(R_c = R) \tag{11}$$

In this development we have neglected those particles which scatter from a surface impurity into nonchanneled directions. These particles will, however, simply join those nonchanneled particles which have

scattered from the surface W atoms and thus there is only a single nonchanneled group.

b) Specific Evaluation of Q_c

As indicated earlier, the limited amount of experimental data presently available do not justify a sophisticated model for the development of the depth distribution function G(R), and thus it seems reasonable to use approximate but realistic values for Q_c in Eq. (1) in order to apply the model to the experimental situation of interest. The Q_c-function given below contains all the qualitative features one would expect in a more sophisticated treatment.

First, it is assumed that if the scattering center lies in a plane of atoms which is parallel to a specific channel then the scattered particle is "blocked" from entering that channel and $Q_c(\theta, \alpha) = 0$ for all θ and α. If the particle is not "blocked" from a particular channel then $Q_c(\theta, \alpha) = Q_{co}$ = constant for all θ, and α, such that the scattered velocity vector is parallel to the channel plane to within $\pm \psi_c$. For scattering events for which this last condition is not satisfied $Q_c = 0$.

To quantify these remarks, let $\hat{u}$ be a unit vector in the original direction of motion, and let $\hat{n}_c$ be the unit normal to the planar channel of interest. Further, let $\hat{s}$ and $\hat{t}$ be unit vectors which, along with $\hat{u}$, form a cartesian coordinate system. The vector $\hat{s}$ is chosen so that $\hat{n}_c$ lies in the u-s plane of the coordinate system. Thus

$$\hat{n}_c = n_{cu}\,\hat{u} + n_{cs}\,\hat{s} \quad . \tag{12}$$

We note that $n_{cu} = \text{Sin}\ \theta_c$ and $n_{cs} = \text{Cos}\ \theta_c$, where θ_c is the angle

between the initial direction of motion and the planar channel c. Let $\hat{q}$ be a unit vector in the direction of the scattered velocity vector. Then, with α measured from the t-axis, $\hat{q}$ is written as

$$\hat{q} = \text{Cos } \theta \; \hat{u} + \text{Sin } \theta \text{ Cos } \alpha \; \hat{t} + \text{Sin } \theta \text{ Sin } \alpha \; \hat{s} \quad . \tag{13}$$

Thus, if ψ is the angle between the scattered velocity vector and the planar channel then

$$\text{Cos}(\pi/2 + \psi) = \hat{q} \cdot \hat{n}_c \tag{14a}$$

$$= n_{cu} \text{Cos } \theta + n_{cs} \text{ Sin } \theta \text{ Sin } \alpha \tag{14b}$$

$$= \text{Sin } \psi \quad . \tag{14c}$$

With the function Q_c described above, and the geometrical relationships of Eqs. (12) - (14), Eq. (1) becomes

$$d\sigma_c(\theta) = Q_{co} \sigma(\theta) \; d(\text{Cos } \theta) \Delta\alpha_c \tag{15}$$

where $\Delta\alpha_c$ is that range of values for α for which $|\psi| \leq \psi_c$, with ψ as determined from Eq. (14).

One can easily see that this model will lead to a peaked structure in the depth distribution as follows. Assume that ψ_c is small, that $\Delta\alpha$ is small, and let α_o be the value of α for which $\psi = 0$, then from (14)

$$4\psi_c = n_{cs} \text{ Sin } \theta \text{ Cos}\alpha_o \; \Delta\alpha, \tag{16}$$

with

$$\text{Sin } \alpha_o = -(n_{cu}/n_{cs}) \text{ Cos } \theta \quad , \tag{17}$$

from which

$$\Delta\alpha = 4\psi_c/(n_{cs}^2 - \text{Cos}^2 \; \theta)^{1/2} \tag{18a}$$

$$\Delta\alpha = 4\psi_c/(\mathrm{Cos}^2\ \theta_c - \mathrm{Cos}^2\ \theta)^{1/2} \quad . \qquad (18b)$$

The extra factor of 2 in Eqs. (16) - (18) results from the two values of α_o which satisfy Eq. (17) for a fixed θ. For $\theta < \theta_c$ the argument in the square root in Eq. (18b) is negative, $\Delta\alpha = 0$, and thus $d\sigma_c$ is zero. For $\pi/2 \geq \theta \geq \theta_c$, $\Delta\alpha$ is a decreasing function of θ with a singularity at $\theta = \theta_c$. Thus, qualitatively, one expects an exact evaluation from Eq. (14) to produce a depth distribution $G_c(R)$ with a sharp peak at a depth corresponding to $\theta = \theta_c$ and with a decreasing tail which extends all the way to R = 0, i.e., the target surface.

From Eqs. (18) it is seen that the magnitude of the peak in the distribution is (roughly) proportional to ψ_c for ψ_c small. What is not so obvious from the above equations is that ψ_c also affects the width of the peak in the distribution. Fig. 3 shows calculated $\Delta\alpha(\theta)$ for several different choices for ψ_c, as a function of Cos θ. The curves have all been normalized to the same peak height to bring out the effect of ψ_c on the predicted peak width. For the curves of Fig. 3, θ_c was chosen as 30^o which for particle incidence along the <110> direction corresponds to (101) planes. From the figure it is seen that the peak widths are an increasing function of ψ_c, and are already quite broad at $\psi_c = 10^o$. A quick comparison of figures 1 and 3 also indicates that the channeling acceptance angles are only a few degrees for those channels represented by the peaks in Fig. 1.

IV. COMPARISON OF EXPERIMENT AND THEORY

Figure 4 shows the predicted depth distribution of those D ions which scatter from surface impurities on a W target, based on the model of the previous section. The surface impurity was assumed to be a carbon atom, its location on the surface was taken such that no planar channels would be "blocked." Further, ψ_c was 1^o for all channels, and the stopping power was assumed the same in all channels with $p_c = 0.5$. The channeling probability constant, Q_{co}, was assumed proportional to $d_c - r_w$ when this quantity was positive, and zero otherwise, where d_c is the interplanar spacing and r_w is the tungsten atom radius defined earlier. A hard sphere cross section $\sigma(\theta)$ was used for these calculations. The scale factor, R_o, on the depth axis is given by $R_o = F_c E^{1/2}$, and it represents the maximum depth which a planar channeled ion can penetrate. Also identified on the figure are the planar channels which contribute to the various peaks displayed there.

Qualitatively, the results shown in Figure 4 will be little changed for other realistic assumptions concerning the parameters which enter the calculations. Increasing the acceptance angle for a given plane will cause the peak associated with that plane to become broader and more prominent. Different assumptions concerning the dependence of Q_{co} on d_c will also change the relative magnitudes of the various peaks, as will the use of a different elastic scattering cross section. Different assumptions concerning the stopping power functions associated with a given plane will change the depth at which the associated peak occurs, as will the use of a different mass surface impurity, although this latter effect is relatively

small for impurities heavier than carbon. Since our present purpose is to point out that the model of Section III can "explain" the structure observed in Fig. 1, and that additional experiments are needed before quantitative results can be confidently extracted from the data, the calculated results displayed in Fig. 4 are entirely adequate.

Comparison of the results in Figs. 1 and 4 allows one to develop a consistent scheme which identifies the various peaks in Fig. 1 with specific planar channels in the W lattice. The results of this comparison, which must be considered as tentative at this time, are shown in Table I. Although the planes which can contribute to each of the experimental peaks are identified in Table I it is not possible to identify with certainty which planes actually do contribute. This is because the magnitudes predicted for the theoretical peaks are relatively sensitive to the assumptions which have been made concerning the parameters Q_c, ψ_c, and σ. The scheme can be used however to evaluate the planar channel stopping powers. The results of this evaluation are shown in Table II. There it is seen that the most open plane, the (110) plane has a stopping power about 15% larger than that of the <110> axis, while all the other planes have stopping power approximately 25 - 35% larger. The uncertainties indicated in the stopping power results in Table II were obtained by assuming that the depth resolution in Fig. 1 is ~ one lattice spacing in the <110> direction. The results indicate that (with the exception of the (102) planes) the stopping powers have a realistic dependence on the planar spacing, d_c. The results for the (102) plane could however be brought into much better agreement with the other data by

simply moving the shallowest peak in Fig. 1 one lattice plane nearer the surface. The planar channel stopping powers are given in Table II as ratios with the stopping power in the <110> axial channel which, with $p_c = 0.5$, is

$$S_{<110>}(eV/\mathring{A}) = 0.179\ E^{1/2}(eV) \quad . \tag{19}$$

The stopping power results in Table II and Eq. (19) represent the first information obtained on dE/dx in this low energy region, previous experiments having been carried out at least an order of magnitude higher in energy. The measured values given here are about a factor of 3 greater than predicted by Lindhard theory, but about a factor of 9 less than predicted by Firsov theory.[7] However, both theories are not strictly applicable to channeled ions.

Thus far attention has been focused primarily on the depth distribution of the implanted D, and the fate of the surface scattering centers has been ignored. The depth distribution of these atoms also carries information, some of which can be extracted using the simple model of Section III. The rich structure observed in Fig. 1 suggests that the surface impurities are located somewhere in the <110> channel at the target surface. Further, estimates of the acceptance angle for C and O channeling along this axis[3] indicate that in all scattering events at the surface the recoiling surface impurity will be confined to the <110> channel. Thus, the channel stopping power for C and O atoms can be extracted from the data of Fig. 1. Assuming that the stopping power is given by Eq. (3) with

$p_c = 0.5$, the resultant stopping powers are

$$S_{<110>}(O)\ (eV/\mathring{A}) = 0.504\ E^{1/2}(eV) \qquad (20a)$$

$$S_{<110>}(C)\ (eV/\mathring{A}) = 0.561\ E^{1/2}(eV) \quad . \qquad (20b)$$

These stopping power values are about a factor of 3 larger than predicted by the Lindhard theory, but about a factor of 3 smaller than predicted by the Firsov theory.[7] Thus the stopping power results for both incident projectiles and the recoiling O and C atoms must be considered to be in as good agreement as can be expected with the theory.

The C and O depth distributions also contain information concerning the elastic scattering cross section σ. An evaluation of σ from these distributions would, of course, have to be consistent with the same evaluation from the D depth distribution, and thus provides a check on the theory. The extraction of σ from the experimental data will have to be postponed, however, until the sophistication of the theoretical model is improved.

V. CONCLUSION

A surface impurity elastic scattering - channeling model has been presented to explain the structure observed in the depth distribution of low energy D implants in (110) tungsten. A consistent scheme identifying the various observed peaks with channeling in various low index crystal planes can be constructed from this model, and channel stopping powers can be extracted from the data using this scheme. The stopping power values obtained fall between the

predictions of two different theories, and thus must be considered as realistic. The model also allows the extraction of the stopping power values for the surface impurities in the <110> channel, since the impurities will recoil down this channel in an elastic scattering event. Again, the values for the stopping powers fall between the predictions of two different theories and are thus realistic. Further refinement of the model is possible, but this refinement should await further experimental measurements which can verify the predictions which the simple model provides. The suggested additional experiments include 1) measurements for D implants for which the neutral component of the beam has been separated to verify the basic assumptions of the model, including the identification of the various contributing planes in Table I, 2) measurement of the D depth distributions over a range of incident energies to verify the energy dependencies of the stopping power, and 3) measurements with targets having "clean" surfaces to verify that the observed effect is indeed due to the impurities.

TABLE I. A Scheme Relating the Peaks in Figure 1 with Planar Channels in the W Target

Peak Depth (atomic layers)	Planar Channels Contributing to Peak
4	Nonchanneled D distribution
11	(102)
13	(103)
16	(112)
19	(111)
22	(100), (103), and (123)
28	(112) and (102)
31	(103)
33	(100), (110), (112), and (103)
37	(112)
46	Axially channeled D along <110> direction

TABLE II. Stopping Powers for Planar Channels Based on Figure 1 and Table I.

Channel	$S_c/S_{<110>}$ [a]	d_c/a [b]
(110)	1.15 ± 0.03	0.71
(100)	1.37 ± 0.14	0.50
(112)	1.29 ± 0.06	0.41
(103)	1.36 ± 0.11	0.32
(111)	1.32 ± 0.06	0.29
(123)	1.28 ± 0.13	0.27
(102)	1.20 ± 0.13	0.22

a. $S_{<110>}(\text{eV/Å}) = 0.179\ E^{1/2}(\text{eV})$.

b. a = lattice constant for W = 3.16 Å.

REFERENCES

1. D. K. Brice, Rad. Effects 11, 227 (1971).
2. J. A. Panitz, J. Vac. Sci. Technol. 14, 502 (1977).
3. J. Lindhard, Kgl. Danske Videnskab. Se skab, Mat.-Fys. Medd. 34, No. 14 (1965); C. Erginsoy, Phys. Rev. Letters 15, 360 (1965).
4. O. S. Oen and M. T. Robinson, Nucl. Inst. and Methods 132, 647 (1976).
5. See, for example Hydrogen Embrittlement of Nonferrous Metals, by B. A. Kolachev (S. Monson Publishers, Jerusalem, 1966) p. 2.
6. P. G. Lucasson and R. M. Walker, Phys. Rev. 127, 485 (1962).
7. J. Lindhard, M. Scharff, and H. E. Schiott, Kgl. Danske Videns[illegible] Selskab, Mat.-Fys. Medd. 33, No. 14 (1963); O. B. Firsov, Zh. Exsperim. i. Teor. Fiz. 36, 1517 (1959). (Sov. Phys. JETP 36 1076 (1959)).
8. See, for example, J. H. Ormrod, J. R. MacDonald, and H. E. Duckworth, Can. J. Phys. 43, 275 (1965).

FIGURE CAPTIONS

Figure 1 (After Panitz, ref. 2) Depth profiles of C^{2+}, C^{+}, O^{+}, and D^{+}, in the near surface region of tungsten, following implantation with 80 eV deuterium at 300 K.

Figure 2 Schematic representation of the channeling model presented in Section III. Incident D ions are shown being scattered into planar channels in the tungsten target by interactions with a monolayer of surface impurity.

Figure 3 Plot of $\Delta\alpha$ versus Cos θ showing the effect of the value of ψ_c on the peak width. Curves have been normalized to the same peak height to emphasize the broadening effect. $\theta_c = 30^{o}$.

Figure 4 Plot of G(R) versus R for the planar channeling model of Section III. For this plot $\psi_c = 1^{o}$, Q_{co} is proportional to planar spacing minus the tungsten atom radius, and the stopping powers in all planar channels are assumed equal and proportional to the square root of the deuterium energy. Also, a hard sphere scattering cross section is used.

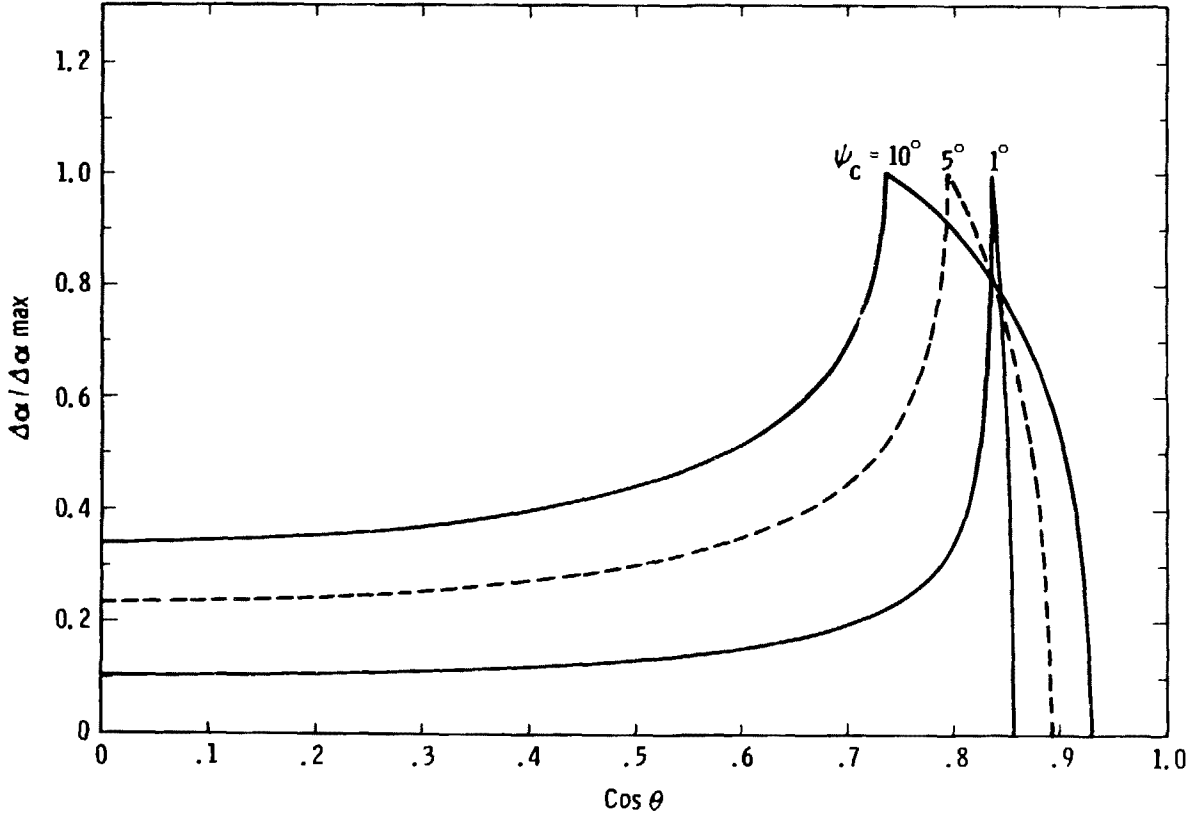

Figure 3

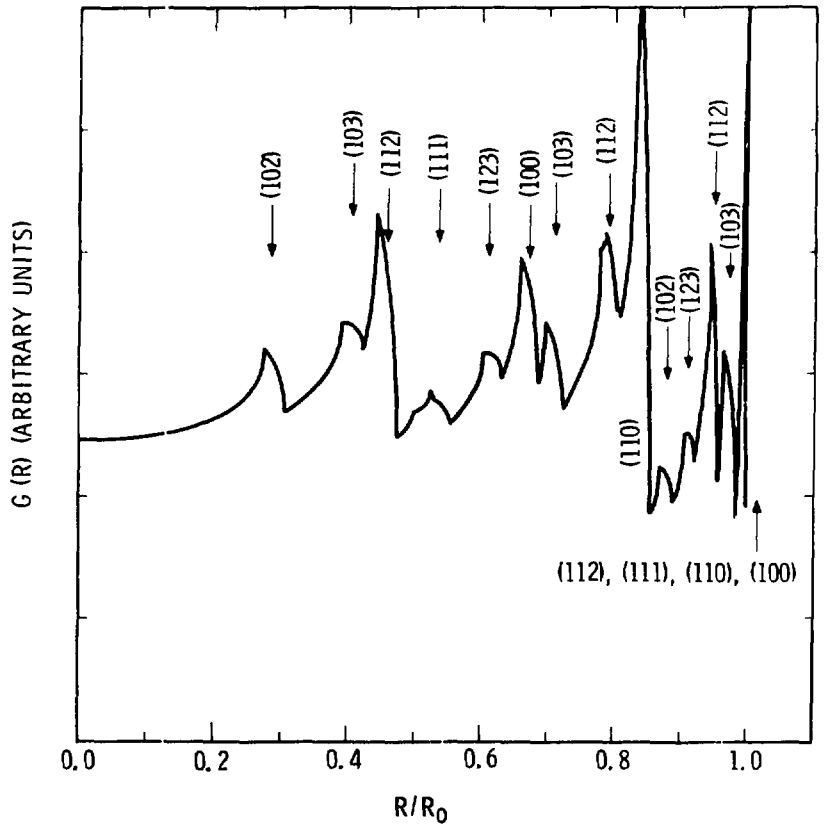
G (R) (ARBITRARY UNITS)
(102)
(103)
(112)
(111)
(123)
(100)
(103)
(112)
(110)
(102)
(123)
(112)
(103)
(112), (111), (110), (100)
0.0
0.2
0.4
0.6
0.8
1.0
R/R0

Figure 4